Dynamics analysis of width-varying microcantilevers: Interplay between eigenfrequencies, contact stiffness and interaction forces

Dynamics analysis of width-varying microcantilevers: interplay between eigenfrequencies, contact stiffness and interaction forces

Nguyen Duy Vy,[1,2,*] Alessio Morelli,[3] Vinh N.T. Pham,[4,5] Dewar Finlay,[3]Amir Farokh Payam[3,+]

[1]*Science and Technology Advanced Institute, Van Lang University, Ho Chi Minh City, Vietnam*

[2]*Faculty of Applied Technology, School of Engineering and Technology, Van Lang University, Ho Chi Minh City, Vietnam*

[3] *School of Engineering, NIBEC, Ulster University, Shore Road, Newtownabbey BT37 0QB, United Kingdom*

[4]*International Cooperation Office, Ho Chi Minh City University of Education, Ho Chi Minh City, Vietnam*

[5]*Department of Physics, Ho Chi Minh City University of Education, Ho Chi Minh City, Vietnam*

[*]*Email: nguyenduyvy@vlu.edu.vn*

[+]*Corresponding author. Email: a.farokh-payam@ulster.ac.uk*

Abstract

In this study, the resonance-frequency dependence and modal sensitivity of the flexural vibration modes of overhang/T-shaped microcantilevers to the interaction force and surface stiffness variations were analysed, and a closed-form expression was derived. The Euler–Bernoulli beam theory was used to develop the overhang/T-shaped models, and a characteristic formula representing the dependence of cantilever frequencies on the overhang dimensions was obtained. The results of the derived expression were analysed using numerical simulations to investigate and compare the effects of the overhang width, length, repulsive and attractive forces, and surface contact stiffness on the flexural mode of overhang/T-shaped cantilevers. Furthermore, a closed-form expression for the modal sensitivities of the width-varying cantilever was derived, and the modal sensitivities were compared using numerical simulations. Finally, the effects of the interaction forces and contact stiffness on the frequency response and sensitivities of different cantilevers based on their stiffness and geometrical parameters were verified experimentally. This study can open new paths for designing, fabricating, and using width-varying cantilevers in sensing and imaging applications, particularly for cantilever array systems.

Introduction

Microcantilevers have been widely used in various technologies, such as actuators in micro-electromechanical systems, sensors, energy harvesters, lab-on-chip technology, and atomic force microscopy (AFM) [1]–[4]. They are used in chemical and biosensing devices to improve

their versatility and detection speed in gas-phase and liquid environments [5]–[9]. In cantilever array sensors, each cantilever is coated with a sensitive layer that can be highly or partially specific to generate response patterns for the molecular recognition of various analytes [8]. In AFM, microcantilevers are utilised to detect minute forces between a sharp probe, typically protruding from the end of a cantilever and the surface of the sample [10]. Recently, functionalized cantilever-probe systems have been used to measure and quantify the physical, chemical, electrical, magnetic, and mechanical properties of an extensive range of materials, from biological objects to composites, polymers, nanoparticles, and even single molecules and atoms [11]–[17]. Platforms of array cantilevers have been developed to overcome the current limitations of AFM to simultaneously determine the multiparametric properties of the surface under study via a single measurement. This can achieve high-resolution multiparametric mapping of the physiochemical properties of the materials [18]–[20].

In array systems, cantilevers are independently actuated or dependently coupled via electrical [21], mechanical [22], or both [23] channels. In exciting and controlling the vibration and response of cantilevers in an array system, the coupling between cantilevers is a crucial factor. Mechanically, the coupling can be achieved by adding a net [24] or full bridge between subsequent cantilevers [22], [25], [26]. This incorporation should be considered during the design and fabrication of single cantilevers used in parallel sensing to tune their properties and dimensions.

In array systems, the overhang that couples subsequent cantilevers can significantly affect the frequency response, particularly for short cantilevers [27], [28]. Hence, an examination of the effect of the overhang on the frequency response of cantilevers is required. Significant efforts have been made to investigate width-varying cantilevers, including T-shaped, overhang-shaped, and trapezoid-shaped cantilevers [27]–[32]. Assuming an analytical function for varying widths, Singh *et al.* [33] derived an equation for calculating the frequency response of width-varying cantilevers. However, the proposed equation is lengthy and complex. Furthermore, there is a lack of a general characteristic equation for the frequency response, and the frequency calculations are based on approximations or numerical results obtained through finite element simulations. In such approximations, the mode shape is assumed to be in the ideal form (a rectangular cantilever), and Rayleigh's energy method is adopted to obtain the resonance frequency [34]. Lan *et al.* [35], derived characteristic equations for the overhang-shaped cantilever when it vibrates freely without any interaction with samples surface while the results being the new equation and the mode shapes as arising from them.

Based on the method proposed in [35], Tri Dat et al [36] developed a methodology to derive the frequency equation and semi-empirical mechanical coupling strength of microcantilevers in an array. However, in these works the cantilever is not in contact with the sample and oscillates freely. When the cantilever is interacted with the sample, the problem becomes complicated as the cantilever has another "effective" spring constant and additional parameters need to be considered.

During AFM operations, the dynamic behaviour of the microcantilevers significantly influences the surface imaging process, affecting the sensitivity and resolution. It is desirable to use the frequency of the most sensitive mode as an excitation frequency for the AFM cantilever to achieve a high image contrast and signal-to-noise ratio (SNR). Several studies have been conducted to analyse the modal sensitivity of AFM cantilevers to variations in surface stiffness in air and liquid environments [3], [37]–[43]. However, the relationship between the frequency response or sensitivity of overhang/T-shaped cantilevers with interaction forces and the effective contact stiffness has not been investigated in detail. In this study, we investigated the dynamic response of overhanging cantilevers to applied forces and the stiffness of the interaction, i.e. the flexural modal sensitivity. This sensitivity is the change of flexural frequency regarding to the flexural vibration, i.e., the vibration normal to the cantilever surface. Changing the interaction force between cantilever and surface of specimen and contact stiffness leads to the change of flexural frequency of cantilever which can be described by flexural modal sensitivity. The flexural modal sensitivity can be normalized by the case of cantilever frequency where there is not contact between cantilever and the surface. The flexural mode is also the most widely used mode in AFM measurements. We derived an analytical closed-form equation to determine the frequency of overhanging cantilevers and another equation to evaluate the sensitivity of overhanging cantilevers to the stiffness of the interaction. Using simulations and experiments, we verified the equations and analysed the frequency response of cantilevers interacting with attractive and repulsive forces for hard and soft materials.

2. Frequency response and modal sensitivity of flexural vibration of overhanging cantilever

The cantilever is represented as a rectangular beam of length l and thickness t, as shown in Figure 1. The overhanging part, with the same thickness t, has length l_0 and width w_0, resulting in the total cantilever length, $L = l + l_0$.

In general, the cantilever involves a sharp tip at the furthest part to interact with the sample. However, this tip is usually fabricated as small as possible to avoid greatly modifying the dynamics of the cantilever. Furthermore, for practical use, the effects of the tip are usually not considered. In the analytical calculation and simulation, the mass and size of the tip could be included at the end part of the cantilever by using an effective mass, or just as a corrected infinitesimal quantity. In the current paper, we assume that the effect of the tip could be omitted, and the cantilever involves the in-plane part only.

Especially, the T-shaped cantilever is usually used to exploit the torsional modes. Therefore, the length of the T part is minimized to ensure that the torsional mode of the main cantilever (excluding the T part) is maintained. Nevertheless, the torsion of the T part should be considered because its length is large (l_0 ~1/3L, Kim et al. [44]). In the current paper, we aim at the change in the frequency of the cantilever due to the size of the T part firstly. The change of the torsional vibrations due to the T-part size could be examined elsewhere. We also changed the size of the T part in a wide range, l_0 from ~0.0 to ~ 1.0 of the total length L. If l_0<0.1L, we will have the T-shaped cantilever as that of Mullin et al. [30] or of Liu et al. [32]. For brevity, in the remainder of the text, we will refer to the above-described kind of cantilevers as width-varying cantilevers, and specifically to overhanging (T-shaped) in case the width at its base is larger (smaller) than at the end.

The Euler–Bernoulli equation is used to model the cantilever and derive the dynamic expressions:

$$m(x)\frac{\partial^2 V(x)}{\partial t^2} = -\frac{\partial^2}{\partial x^2}\left[EI(x)\frac{\partial^2 V(x)}{\partial x^2}\right] \tag{1}$$

where $V(x,t)$ is the deflection at x and time t, $m(x)$ is the mass per unit length, and E and $I(x)$ are the (elastic) Young's modulus and the area moment of inertia of the cross-section, respectively. Using the separation of variables method, $V(x,t) = W(x)G(t)$, we obtain the following expressions:

$$\frac{1}{G(t)}\frac{d^2G(t)}{dt^2} = -\frac{1}{m(x)W(x)}\frac{d^2}{dx^2}\left[EI(x)\frac{d^2W(x)}{dx^2}\right]$$

$$\Leftrightarrow \begin{cases} \dfrac{d^2G(t)}{dt^2} + \omega^2 G(t) = 0 \\ \dfrac{d^2}{dx^2}\left[EI(x)\dfrac{d^2W(x)}{dx^2}\right] - m(x)\omega^2 W(x) = 0 \end{cases}. \tag{2}$$

The first part of Eq. (2) implies a periodic oscillation with frequency ω. When the cantilever has a rectangular shape (without an overhang) and exhibits uniform mechanical properties along its length, $I(x)$ is independent of x.

Based on the above equations and mathematical calculations, the following characteristic equation is derived [See the Supplementary Information for further details]:

$$C(\beta, k_f, l, l_0, \kappa)=4 + 4\kappa^2 + (1 + 6\kappa + \kappa^2)cos\beta cosh\beta + 4(-1 + \kappa^2)cos\beta\eta cosh\beta\eta - 4cos[\beta - \beta\eta]cosh[\beta - \beta\eta] + 4\kappa^2\, cos[\beta - \beta\eta]cosh[\beta - \beta\eta] + (1 - \kappa)^2(2cos[\beta\eta]cos[\beta - \beta\eta]cosh[\beta - 2\beta\eta] + cos[\beta - 2\beta\eta]cosh[\beta]) + \frac{\left(\frac{1}{2}+\frac{i}{2}\right)\nu}{\beta^3}\Big((1 + 6\kappa + \kappa^2) \times \left(\sin\big((1 + i)\beta\big) - sinh\big((1 + i)\beta\big)\right) + (1 - \kappa)^2 \times \left(sin\left(\beta\big((1 + i) - 2\eta\big)\right) - sinh\left(\beta\big((1 + i) - 2\eta\big)\right)\right) + (1 - \kappa)^2 \times \left(sin\left(\beta\big((1 + i) - 2i\eta\big)\right) - sinh\left(\beta\big((1 + i) - 2i\eta\big)\right)\right) + 4(1 - \kappa^2) \times \big(sin((1 + i)\beta(-1 + \eta)) - sinh((1 + i)\beta(-1 + \eta))\big) + (1 - i)(1 - \kappa)^2 \times \big(cosh(\beta - 2\beta\eta)sin(\beta - 2\beta\eta) - cos(\beta - 2\beta\eta)sinh(\beta - 2\beta\eta)\big)\Big), \quad (3)$$

where $\eta = l_0/L$. The eigenvalues of the overhanging cantilever were obtained using the characteristic equation above. Therefore, the eigenvalues for the frequency are functions of l_0 and κ, as $\beta = \beta(l_0, \kappa)$. For the case without an overhang, $l_0 = 0$. The frequency for the cantilever with overhangs is defined as follows.

$$\omega_i = \beta_i^2\sqrt{EI/M} \quad (4)$$

Note that I and M in Eq. (4) correspond to the cantilever body $\{l, w\}$ as $I/M = I_0/M_0$. To calculate the sensitivity of the overhanging microcantilever to surface stiffness–force interaction, we used the equation

$$\frac{\partial\omega_n}{\partial\nu} = \frac{\partial\omega_n}{\partial\beta}\frac{\partial\beta}{\partial\nu}\ . \quad (5)$$

$\frac{\partial\omega_n}{\partial\beta}$ can be calculated as follows.

$$\frac{\partial\omega_n}{\partial\beta} = 2\beta_n\sqrt{\frac{EI}{M}}\ . \quad (6)$$

From Eq. (3), we obtain the following equations:

$$\frac{\partial\beta}{\partial\nu} = -\frac{\partial C/\partial\nu}{\partial C/\partial\beta}, \quad (7)$$

$$\frac{\partial C}{\partial \nu} = \frac{\left(\frac{1}{2}+\frac{i}{2}\right)}{\beta^3}\Big((1+6\kappa+\kappa^2)\times\left(\sin\big((1+i)\beta\big)-sinh\big((1+i)\beta\big)\right)+(1-\kappa)^2\times$$
$$\left(sin\left(\beta\big((1+i)-2\eta\big)\right)-sinh\left(\beta\big((1+i)-2\eta\big)\right)\right)+(1-\kappa)^2\times\left(sin\left(\beta\big((1+i)-$$
$$2i\eta\big)\right)-sinh\left(\beta\big((1+i)-2i\eta\big)\right)\right)+4(1-\kappa^2)\times\big(sin((1+i)\beta(-1+\eta))-$$
$$sinh((1+i)\beta(-1+\eta))\big)+(1-i)(1-\kappa)^2\times\big(cosh(\beta-2\beta\eta)sin(\beta-2\beta\eta)-$$
$$cos(\beta-2\beta\eta)sinh(\beta-2\beta\eta)\big)\Big), \qquad (8)$$

$$\frac{\partial C}{\partial \beta} = (1+6\kappa+\kappa^2)(cos\beta sinh\beta - sin\beta cosh\beta)+4\eta(\kappa^2-1)(sinh\beta\eta cos\beta\beta\eta -$$
$$sin\beta\eta cosh\beta\eta)+4(\kappa^2-1)(1-\eta)\big(cos(\beta-\beta\eta)sinh(\beta-\beta\eta)-sin(\beta-\beta\eta)cosh(\beta-$$
$$\beta\eta)\big)+(1-\kappa)^2(-2\eta sin(\beta\eta)cos(\beta-\beta\eta)cosh(\beta-\beta\eta)-2(1-\eta)cos(\beta\eta)sin(\beta-$$
$$\beta\eta)cosh(\beta-2\beta\eta)+2(1-2\eta)cos(\beta\eta)cos(\beta-\beta\eta)sinh(\beta-2\beta\eta)+cos(\beta-$$
$$2\beta\eta)sinh\beta-(1-2\eta)sin(\beta-2\beta\eta)cosh\beta)-\frac{3\left(\frac{1}{2}+\frac{i}{2}\right)\nu}{\beta^4}\Big((1+6\kappa+\kappa^2)\times\left(\sin\big((1+i)\beta\big)-$$
$$sinh\big((1+i)\beta\big)\right)+(1-\kappa)^2\times\left(sin\left(\beta\big((1+i)-2\eta\big)\right)-sinh\left(\beta\big((1+i)-2\eta\big)\right)\right)+$$
$$(1-\kappa)^2\times\left(sin\left(\beta\big((1+i)-2i\eta\big)\right)-sinh\left(\beta\big((1+i)-2i\eta\big)\right)\right)+4(1-\kappa^2)\times$$
$$\left(sin\big((1+i)\beta(-1+\eta)\big)-sinh\big((1+i)\beta(-1+\eta)\big)\right)+(1-i)(1-\kappa)^2\times$$
$$\big(cosh(\beta-2\beta\eta)sin(\beta-2\beta\eta)-cos(\beta-2\beta\eta)sinh(\beta-2\beta\eta\eta)\big)\Big)+\frac{\left(\frac{1}{2}+\frac{i}{2}\right)\nu}{\beta^3}\Big((1+6\kappa+$$
$$\kappa^2)\times\big((1+i)(\cos(\beta(1+i))-\cosh(\beta(1+i))\big)+(1-\kappa)^2\times\Big(\big((1+i)-$$
$$2\eta\big)\left(\cos\left(\beta\big((1+i)-2\eta\big)-\cosh\left(\beta\big((1+i)-2\eta\big)\right)\right)\right)+(1-\kappa)^2\times\big((1+i)-$$
$$2i\eta\big)\left(\cos\left(\beta\big((1+i)-2i\eta\big)-\cosh\big(\beta\big((1+i)-2i\eta\big)\right)+4(1-\kappa^2)\times(1+i)(-1+\right.$$
$$\eta)(\cos(\beta(1+i)(-1+\eta))-\cosh\big(\beta(1+i)(-1+\eta)\big)+(1-i)\times(1-\kappa)^2\times$$
$$\big((1-2\eta)sinh(\beta-2\beta\eta)sin(\beta-2\beta\eta)+(1-2\eta)cosh(\beta-2\beta\eta)cos(\beta-2\beta\eta)+$$
$$(1-2\eta)sin(\beta-2\beta\eta)sinh(\beta-2\beta\eta)-(1-2\eta)cos(\beta-2\beta\eta)cosh(\beta-2\beta\eta)\big)\Big).$$

(9)

Substituting Eqs. (8) and (9) into Eq. (7) yields $\frac{\partial \beta}{\partial \nu}$.

3. Materials and Methods

In this section, simulation and experimental results are presented and discussed. For the simulations, we selected the following parameters: $L = 200\ \mu m$, $w = 20\ \mu m$, $t = 0.8\ \mu m$, $E = 250\ GPa$, and $\rho = m/L = 3100\ kg/m^3$ while $\eta = l_0/L$, $\kappa = w/w_0$ and ν (interaction force) have been varied to predict the behaviour of the resonance frequency modes (normalized to ω/ω_0 where ω_0 is free resonance frequency) and sensitivity in relation to these physical variables. Note that all the simulation results for the frequency analysis are based on normalized frequencies.

Two samples of materials with significantly different Young's moduli were employed to experimentally validate the simulation results: polystyrene (PS, Agar Scientific, E ≈ 4.5 GPa) and silicone elastomer (SE, Goodfellow, E ≈ 50 MPa). The experiments were performed in air using a commercial AFM system (D3100 Nasoscope III Digital Instruments, now Bruker) in amplitude-modulation AFM (AM-AFM, tapping mode) with overhanging silicon probes for tapping mode SCOUT70 (spring constant = 2 Nm^{-1}, resonance frequency = 70 kHz, and radius of curvature < 10 nm) and SCOUT350 (42 Nm^{-1}, 350 kHz, <10 nm) (Nu Nano Ltd.).

The microcantilevers were imaged by Scanning Electron Microscopy (SEM – SU5000 Hitachi) in low pressure environment (50 Pa) with a 30 kV acceleration voltage, by use of the Backscattered Electron detector.

For each cantilever and sample, two separate sets of experiments were performed in the AM-AFM mode by tuning the first and second resonance frequencies with a target root-mean-square amplitude of 1 V. After engaging, frequency sweeps were performed to record the variation in the resonance frequency and shape of the resonance peak at set lift heights from 100 nm (minimal tip–sample interaction) to negative values until the resonance peak disappeared (the tip adhering to the surface of the sample). The lift height was relative to the average tip-sample distance in the AM-AFM mode at the established setpoint.

4. Results and discussion

4.1 Analytical results

The frequency response of different eigenfrequencies of microcantilever with different overhang width and length has been seen to be significantly dependent on either attractive or repulsive interaction forces. The higher the mode order, the stronger the dependence is seen. The effect of repulsive force on overhanging cantilevers ($\kappa<1$) is more significant than T-shaped ones ($\kappa>1$). However, there is a direct relation between increase of repulsive force and

frequency of all modes. From the results it can be summarized that the effect of interaction force on overhanging cantilever and lower modes is higher than on T-shaped cantilever and higher modes. [See the Supplementary Information for more details].

To investigate the effect of the overhang length and width under the same repulsive force, we set two different lengths and varied the width of the overhanging part. As shown in Figure 2a and b, an increase in η decreases the frequency. For the same η, an increase in κ increases the frequency of the first three eigenmodes, whereas the fourth eigenmode exhibits nonlinear behaviour, indicating a nonlinear relationship between frequency, η, and κ. Similarly, the variation in frequency with interaction force for a set η on overhang ($\kappa = 0.5$) and T-shaped ($\kappa = 1.5$) cantilevers was analysed (Figure 2c and d). A nonlinear relationship between the frequencies and forces for both cantilevers is evident. For the overhanging cantilever, frequency peaks appear at different applied force values for different modes, and the frequency shift for the lower eigenmodes is higher than that for higher eigenmodes. The frequency response of T-shaped cantilevers is the inverse of that of the overhang cantilevers. An increase in the force decreased the frequency until the trough point was reached, after which the frequency increased again. However, the frequency sensitivity of the T-shaped cantilevers follows the same trend as that of the overhang cantilevers, with a more significant change for the lower modes.

The effect of η for the T-shaped and overhang cantilevers with free vibration ($\nu = 0$) and repulsive force ($\nu > 0$) is shown by the simulation results in Figure 3. In the case of free vibration, the frequency response is symmetric for all modes. Nonlinear behaviour of the modes with respect to each other is observed, indicating that for a η value of approximately 0.5, the frequency of the third mode is higher than that of the fourth mode. Furthermore, for the length of the overhang equal to the main body length of the cantilever ($\eta = 0.5$), the first resonance frequency of the overhanging beam is at its lowest value, whereas the third eigenfrequency is at its highest frequency (Figure 3a). Under a repulsive force (Figure 3b), the frequency response is entirely nonlinear, with the highest frequencies occurring at $\eta = 1$. For a freely vibrating T-shaped cantilever, the frequency response is also symmetric; however, at $\eta = 0.5$, the highest frequency value occurs only in the first mode. In the case of the repulsive force ($\nu = 100$) (Figure 3d), the frequency response of all modes is nonlinear, with varying η under the lowest frequency for each eigenmode at $\eta = 1$.

Several simulations were performed to study the sensitivity of width-varying T-shaped cantilevers to surface stiffness. The width ratio was set to $\kappa = 1.5$ to study the effect of the overhang length on the modal sensitivity of the cantilever, and the sensitivity with varying stiffness was calculated for different values of η, (Figure 4).

A nonlinear relationship between the stiffness, η, and sensitivity is evident. In the first mode, an increase in η decreased the sensitivity, whereas, in higher modes, the behaviour is different. In the second mode, the most sensitive case was associated with $\eta = 0.6$, with $\eta = 1$ yielding the lowest sensitivity. In the third and fourth modes, $\eta = 0.8$ resulted in the highest sensitivity, but the order of modes for other length ratios was not the same. However, the general trend of rectangular cantilevers can be observed for decreased sensitivity with respect to stiffness, with the first mode being the most sensitive for soft surfaces and higher modes more sensitive to stiffer surfaces.

A similar analysis was performed for overhanging cantilevers (Figure 5). In this case, the sensitivity of the first mode was inversely proportional to that of the T-shaped cantilevers. The highest sensitivity occurred at $\eta = 1$, and a decrease in η resulted in decreased sensitivity. In higher modes, the behaviour is more complex, with the highest sensitivity at $\eta = 1$ for soft materials (in other words, for low repulsive force), similar as for the first mode. Under high repulsive force, $\eta = 1$ yields the lowest sensitivity.

Finally, the simulation results for the effect of the cantilever width are presented in Figure 6. All the modes exhibited similar behaviour, and a linear relationship between κ and sensitivity was observed. The results show that increasing the width leads to decreased sensitivity. Moreover, by increasing the surface stiffness, the higher modes would be more sensitive than the lower modes.

4.2. Experimental results

To analyse and compare the frequency responses of cantilevers to the interaction force and contact stiffness for soft and hard materials, we considered two different cantilevers (stiff and soft) and two different samples: SE as the soft material (E ≈ 10 MPa) and PS as the hard material (E ≈ 3 GPa). Cantilever's dimensions were measured by SEM (Figure 7), yielding equal width factor $\kappa = 0.141$ and length factor $\eta = 0.262$, $\eta = 0.365$ for the Scout70 (Figure7a) and Scout350 (Figure7b) cantilever, respectively.

We should mention the changes in frequencies and sensitivities when changing κ and η (=l0/L) of different types of cantilevers come directly from the change of parameters. As a result, the

model and analytical results are consistent and thorough with κ and η. The T-shaped differ to the overhang-shaped cantilevers just in the values of κ. So, the experimental results for the T-shaped cantilevers, could be inferred from the ones for overhang-shaped cantilevers. So, in this work, for the experiments we just focus on overhang-shaped cantilevers as they are commercially more available in market.

Figure 8 shows the frequency response of the first mode with cantilever approaching the sample's surface at different lift heights. Given that the lift height changes the average tip-surface distance during AM-AFM, a positive (negative) lift height results in reduced (increased) effective contact stiffness as described in [43]. As the results show, approaching the cantilever towards the surface of the sample leads to changes in curves' amplitude. For both cantilevers the effect on the amplitude of the frequency curve is more significant on PS than on elastomer.

The second eigenfrequency response of the cantilevers are depicted in Figure 9. Sensitivity and frequency shifts of both cantilevers are higher on polystyrene than on elastomer, and the effect of soft surface on the second mode is less significant than on the first mode, as predicted by our analytical model and simulations.

Finally, we simulated the overhang-shape cantilever with the parameters of SCOUT70 cantilever in interaction with ES and PS. Figure 10, displaying ω/ω_0 vs calculated normalised contact stiffness ν for results from soft cantilever on both materials, show agreement with simulation results (with width and length factors closer to the cantilever's ones). Due to the low Young's modulus of the soft material (Figure 10a), the resulting stiffness range for varying surface distance lies at very low values, with corresponding ω/ω_0 showing little variations, matching the trend predicted by simulations for low ν for the first mode. The behaviour of first eigenfrequency for the hard material shows a plateau and a decline, similar to the one predicted by simulations for the first mode in the same range of ν (Figure 10b).

Furthermore, for the second eigenfrequency, ω/ω_0 vs calculated normalised contact stiffness ν for results from soft cantilever (Figures 10c and d), show again agreement with the trends shown by simulations, with flat profile for soft material (low ν) and ascending slope for hard material ($\nu > 20$).

5. Conclusion

In this study, the Euler–Bernoulli beam theory was used to model and analyse the frequency response and modal sensitivities of overhanging/T-shaped cantilevers. Closed-form

expressions were derived for the resonance frequencies of width-varying microcantilevers. An analytical equation for the flexural sensitivity of such cantilevers to variations in the specimen surface stiffness and interaction forces is proposed. For lower values of normal stiffness, the first mode is the most sensitive; however, as the stiffness increases, higher modes become more sensitive.

The results show a nonlinear relationship between the overhang width, length, interaction forces, and surface contact stiffness. Using experiments on two cantilevers and two samples with different stiffness values, we analysed the effects of the interaction force and sample stiffness on the microcantilevers based on AFM. The experimental data either qualitatively or quantitatively validated the proposed method and simulation results. Our results enable a predictive design in fabricating overhang microcantilevers for applications in sensing and imaging mechanisms. Moreover, our experiments and simulations can help AFM users select appropriate cantilevers and excitation mechanisms to obtain higher SNRs and resolutions, depending on the sample under study. Finally, our developed methodology can be extended to study the behaviour of overhanging cantilevers in liquid environment by considering the effect of hydrodynamic function in liquid environment.

Acknowledgements

AFP, AM, and DF acknowledge the support of the Research Recovery Fund provided by the Northern Ireland Department for Economy (DfE).

References

[1] H. Etayash, M. F. Khan, K. Kaur, and T. Thundat, “Microfluidic cantilever detects bacteria and measures their susceptibility to antibiotics in small confined volumes,” *Nat. Commun.*, vol. 7, pp. 1–9, 2016.

[2] K. Li, Q. He, J. Wang, Z. Zhou, and X. Li, “Wearable energy harvesters generating electricity from low-frequency human limb movement,” *Microsystems Nanoeng.*, vol. 4, no. 1, 2018.

[3] V. V. Korolkov *et al.*, “Ultra-high resolution imaging of thin films and single strands of polythiophene using atomic force microscopy,” *Nat. Commun.*, vol. 10, no. 1, pp. 1–8, 2019.

[4] M. Dukic *et al.*, “Direct-write nanoscale printing of nanogranular tunnelling strain sensors for sub-micrometre cantilevers,” *Nat. Commun.*, vol. 7, pp. 1–7, 2016.

[5] L. Duraffourg and J. Arcamone, “Nanoelectromechanical Systems,” *Nanoelectromechanical Syst.*, vol. 290, no. November, pp. 1–197, 2015.

[6] E. A. Wachter and T. Thundat, “Micromechanical sensors for chemical and physical measurements,” *Rev. Sci. Instrum.*, vol. 66, no. 6, pp. 3662–3667, 1995.

[7] R. Berger, E. Delamarche, H. P. Lang, C. Gerber, J. K. Gimzewski, and E. Meyer, “Surface Stress in the Self-Assembly of Alkanethiols on Gold Surface Stress in the Self-Assembly of Alkanethiols on Gold Ru,” *Appl. Phys. A Mater. Sci. Process.*, vol. 2021, no. 1997, pp. 55–59, 2007.

[8] H. P. Lang, M. Hegner, and C. Gerber, “Cantilever array sensors,” *Mater. Today*, vol. 8, no. 4, pp. 30–36, 2005.

[9] R. Berger *et al.*, “Surface stress in the self-assembly of alkanethiols on gold,” *Science (80-.).*, vol. 276, no. 5321, pp. 2021–2024, 1997.

[10] A. Raman, J. Melcher, and R. Tung, “Cantilever dynamics in atomic force microscopy,” *Nano Today*, vol. 3, no. 1–2, pp. 20–27, 2008.

[11] D. Martin-Jimenez, A. Ihle, S. Ahles, H. A. Wegner, A. Schirmeisen, and D. Ebeling, “Bond-level imaging of organic molecules using Q -controlled amplitude modulation atomic force microscopy,” *Appl. Phys. Lett.*, vol. 117, no. 13, 2020.

[12] D. Alsteens, H. E. Gaub, R. Newton, M. Pfreundschuh, C. Gerber, and D. J. Müller, “Atomic force microscopy-based characterization and design of biointerfaces,” *Nat. Rev. Mater.*, vol. 2, no. 5, pp. 1–16, 2017.

[13] D. Alsteens *et al.*, “Imaging G protein-coupled receptors while quantifying their ligand-binding free-energy landscape,” *Nat. Methods*, vol. 12, no. 9, pp. 845–851, 2015.

[14] R. Garcia, “Nanomechanical mapping of soft materials with the atomic force microscope: Methods, theory and applications,” *Chem. Soc. Rev.*, vol. 49, no. 16, pp. 5850–5884, 2020.

[15] C. Cafolla, W. Foster, and K. Voïtchovsky, “Lubricated friction around nanodefects,” *Sci. Adv.*, vol. 6, no. 14, pp. 1–9, 2020.

[16] N. Bhalla, Y. Pan, Z. Yang, and A. F. Payam, “Opportunities and Challenges for Biosensors and Nanoscale Analytical Tools for Pandemics: COVID-19,” *ACS Nano*,

2020.

[17] A. F. Payam, A. Morelli, and P. Lemoine, “Multiparametric analytical quantification of materials at nanoscale in tapping force microscopy,” *Appl. Surf. Sci.*, vol. 536, no. July 2020, p. 147698, 2021.

[18] W. Shim, K. A. Brown, X. Zhou, B. Rasin, X. Liao, and C. A. Mirkin, “Multifunctional cantilever-free scanning probe arrays coated with multilayer graphene,” *Proc. Natl. Acad. Sci. U. S. A.*, vol. 109, no. 45, pp. 18312–18317, 2012.

[19] Q. Yang *et al.*, “Array atomic force microscopy for real-time multiparametric analysis,” *Proc. Natl. Acad. Sci. U. S. A.*, vol. 116, no. 13, pp. 5872–5877, 2019.

[20] W. Cao, N. Alsharif, Z. Huang, A. E. White, Y. H. Wang, and K. A. Brown, “Massively parallel cantilever-free atomic force microscopy,” *Nat. Commun.*, vol. 12, no. 1, pp. 1–7, 2021.

[21] S. Krylov, S. Lulinsky, B. R. Ilic, and I. Schneider, “Collective dynamics and pattern switching in an array of parametrically excited micro cantilevers interacting through fringing electrostatic fields,” *Appl. Phys. Lett.*, vol. 105, no. 7, 2014.

[22] H. Yabuno, Y. Seo, and M. Kuroda, “Self-excited coupled cantilevers for mass sensing in viscous measurement environments,” *Appl. Phys. Lett.*, vol. 103, no. 6, 2013.

[23] M. Napoli, W. Zhang, K. Turner, and B. Bamieh, “Characterization of electrostatically coupled microcantilevers,” *J. Microelectromechanical Syst.*, vol. 14, no. 2, pp. 295–304, 2005.

[24] G. Cai and Z. Rui, “Net -overhang Coup pled Microcantilevers fo or Sensitive Mass Detection,” in *Proceedings of SENSORS, 2013 IEEE*, 2013, vol. 1, no. 1, pp. 2–5.

[25] S. Marquez, M. Alvarez, J. A. Plaza, L. G. Villanueva, C. Dominguez, and L. M. Lechuga, “Asymmetrically coupled resonators for mass sensing,” *Appl. Phys. Lett.*, vol. 111, no. 11, 2017.

[26] T. Chopard, V. Lacour, and T. Leblois, “GaAs coupled micro resonators with enhanced sensitive mass detection,” *Sensors (Switzerland)*, vol. 14, no. 12, pp. 22785–22797, 2014.

[27] S. Guillon *et al.*, “Effect of non-ideal clamping shape on the resonance frequencies of silicon nanocantilevers,” *Nanotechnology*, vol. 22, no. 24, 2011.

[28] L. Fadel-Taris *et al.*, “Influence of non-ideal clamping in microcantilever resonant frequency estimation,” *Proc. IEEE Int. Freq. Control Symp. Expo.*, pp. 1–5, 2011.

[29] O. Sahin, C. F. Quate, O. Solgaard, and A. Atalar, “Resonant harmonic response in tapping-mode atomic force microscopy,” *Phys. Rev. B - Condens. Matter Mater. Phys.*, vol. 69, no. 16, pp. 1–9, 2004.

[30] N. Mullin, C. Vasilev, J. D. Tucker, C. N. Hunter, C. H. M. Weber, and J. K. Hobbs, “‘torsional tapping’ atomic force microscopy using T-shaped cantilevers,” *Appl. Phys. Lett.*, vol. 94, no. 17, pp. 16–19, 2009.

[31] K. Mohamed, H. Elgamal, and S. A. Kouritem, “An experimental validation of a new shape optimization technique for piezoelectric harvesting cantilever beams,” *Alexandria Eng. J.*, vol. 60, no. 1, pp. 1751–1766, 2021.

[32] Y. Liu, K. M. Leung, H. Y. Nie, W. M. Lau, and J. Yang, “A new AFM nanotribology method using a T-shape cantilever with an off-axis tip for friction coefficient measurement with minimized Abbé error,” *Tribol. Lett.*, vol. 41, no. 1, pp. 313–318, 2011.

[33] S. S. Singh, P. Pal, and A. K. Pandey, “Pull-in analysis of non-uniform microcantilever beams under large deflection,” *J. Appl. Phys.*, vol. 118, no. 20, 2015.

[34] J. Tamayo, D. Ramos, J. Mertens, and M. Calleja, “Effect of the adsorbate stiffness on the resonance response of microcantilever sensors,” *Appl. Phys. Lett.*, vol. 89, no. 22, pp. 4–7, 2006.

[35] L. T. Dat, N. D. Vy, and V. Lan, “Exact mode shapes of T-shaped and overhang-shaped microcantilevers,” *Commun. Phys.*, vol. 30, no. 3, pp. 301–310, 2020.

[36] L. T. Dat, V. N. T. Pham, N. D. Vy, and A. F. Payam, “Frequency equation and semi-empirical mechanical coupling strength of microcantilevers in an array,” *Microsc. Res. Tech.*, vol. 85, no. 9, pp. 3237–3244, 2022.

[37] J. A. Turner and J. S. Wiehn, “Sensitivity of flexural and torsional vibration modes of atomic force microscope cantilevers to surface stiffness variations,” *Nanotechnology*, vol. 12, no. 3, pp. 322–330, 2001.

[38] W. J. Chang, “Sensitivity of vibration modes of atomic force microscope cantilevers in continuous surface contact,” *Nanotechnology*, vol. 13, no. 4, pp. 510–514, 2002.

[39] A. F. Payam and M. Fathipour, “Effect of tip mass on frequency response and sensitivity of AFM cantilever in liquid,” *Micron*, vol. 70, pp. 50–54, Mar. 2015.

[40] A. F. Payam, “Sensitivity of flexural vibration mode of the rectangular atomic force microscope micro cantilevers in liquid to the surface stiffness variations,” *Ultramicroscopy*, vol. 135, pp. 84–88, Dec. 2013.

[41] A. F. Payam, “Sensitivity analysis of vibration modes of rectangular cantilever beams immersed in fluid to surface stiffness variations,” *Sci. Iran.*, vol. 20, no. 4, pp. 1221–1227, 2014.

[42] A. F. Payam and N. D. Vy, “Dynamic analysis of flexural vibration mode of an atomic force microscope cantilever with a sidewall probe in liquid,” *Microsc. Res. Tech.*, no. September, pp. 1–7, 2020.

[43] A. F. Payam and M. Fathipour, “Study of the tip mass and interaction force effects on the frequency response and mode shapes of the AFM cantilever,” *Int J Adv Manuf Technol*, pp. 957–966, 2013.

[44] Y. Kim, N. Mandriota, D. Goodnight, and O. Sahin, “Calibration of T-shaped atomic force microscope cantilevers using the thermal noise method,” *Rev. Sci. Instrum.*, vol. 91, no. 8, 2020.

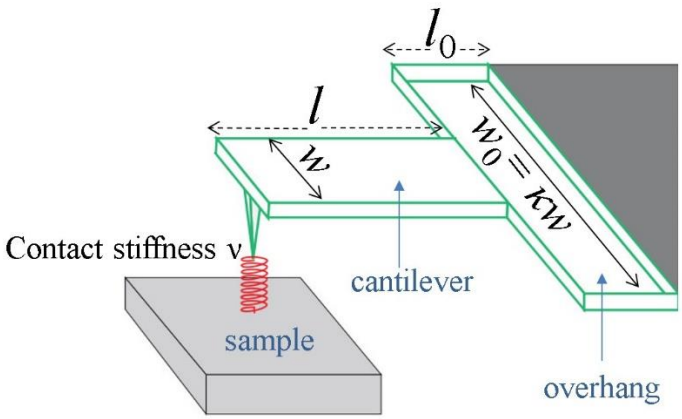

Figure 1. Models of microcantilevers: a cantilever with an overhanging part of length l_0 and width w_0. The length and width of the main body of the cantilever are l and w, respectively. We define $\eta = l_0/(l_0 + l)$ and $\kappa = w/w_0$. For $w_0 < w$, a T-shaped cantilever is defined.

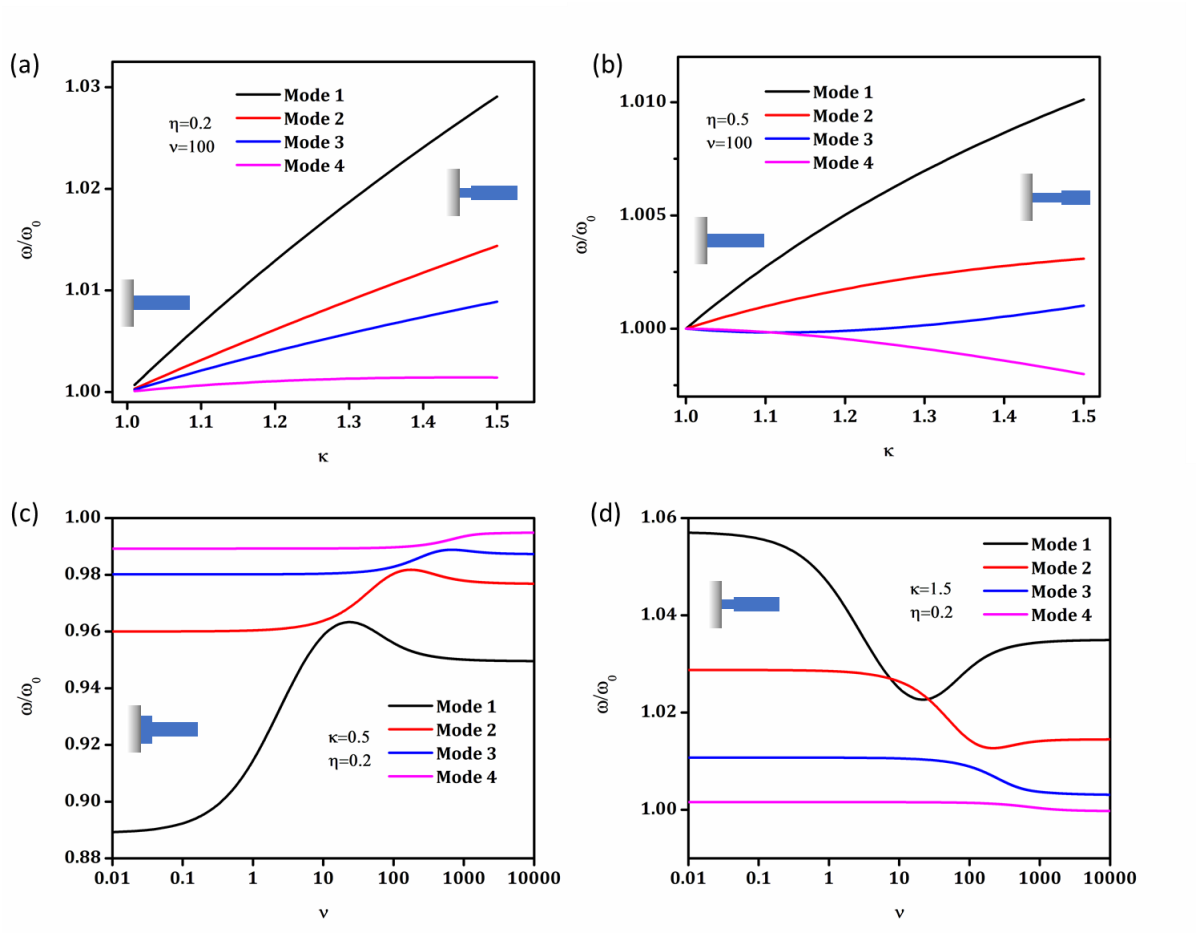

Figure 2. Frequency response of a) T-shaped cantilever with $\eta = 0.2$ and b) $\eta = 0.5$ and same contact stiffness to varying overhang width. c) Frequency response of overhanging cantilever with $\eta = 0.2$ to varying repulsive force and contact stiffness. d) Frequency response of T-shaped cantilever with $\eta = 0.2$ to varying repulsive force and contact stiffness.

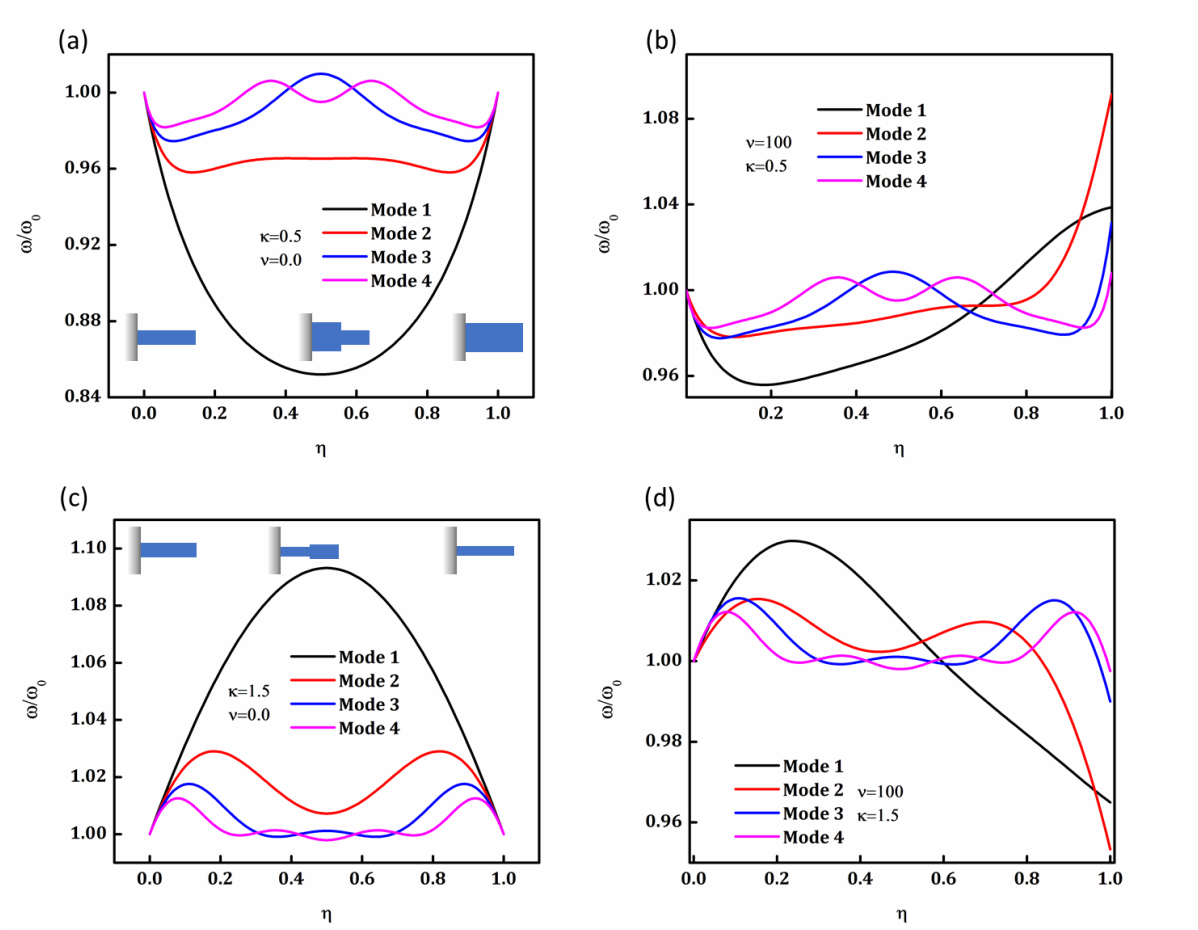

Figure 3. Frequency response of a) freely vibrated overhanging cantilever with $\kappa = 0.5$ and b) overhanging cantilever with $\kappa = 0.5$ and $\nu = 100$ (repulsive force) to variation in overhang length. Frequency response of c) freely vibrated T-shaped cantilever with $\kappa = 1.5$, and d) T-shaped cantilever with $\kappa = 1.5$ and $\nu = 100$ (repulsive force) to variation in overhang length.

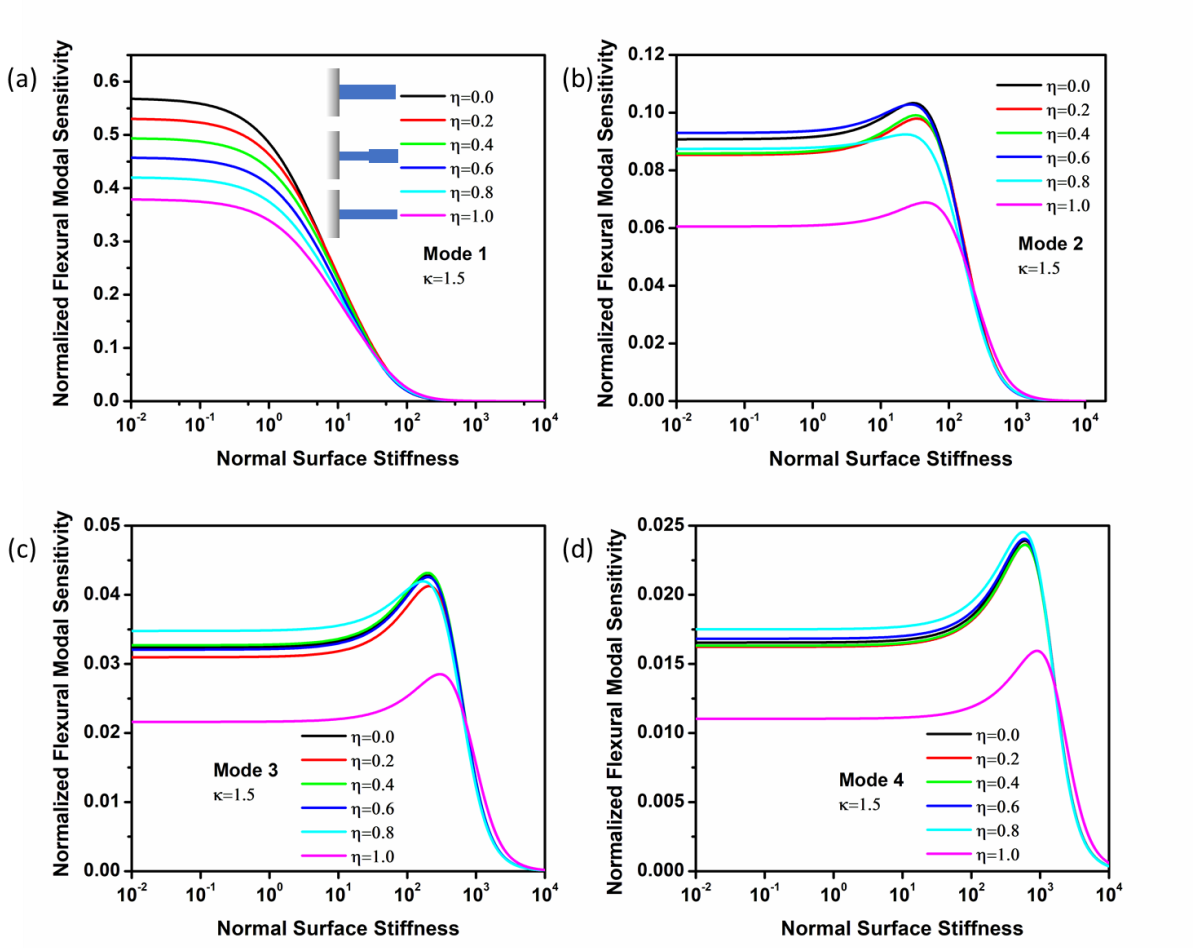

Figure 4. Flexural modal sensitivity of T-shaped cantilever ($\kappa = 1.5$) as function of normal contact stiffness and overhanging length for a) first mode, b) second mode, c) third mode, and d) fourth mode.

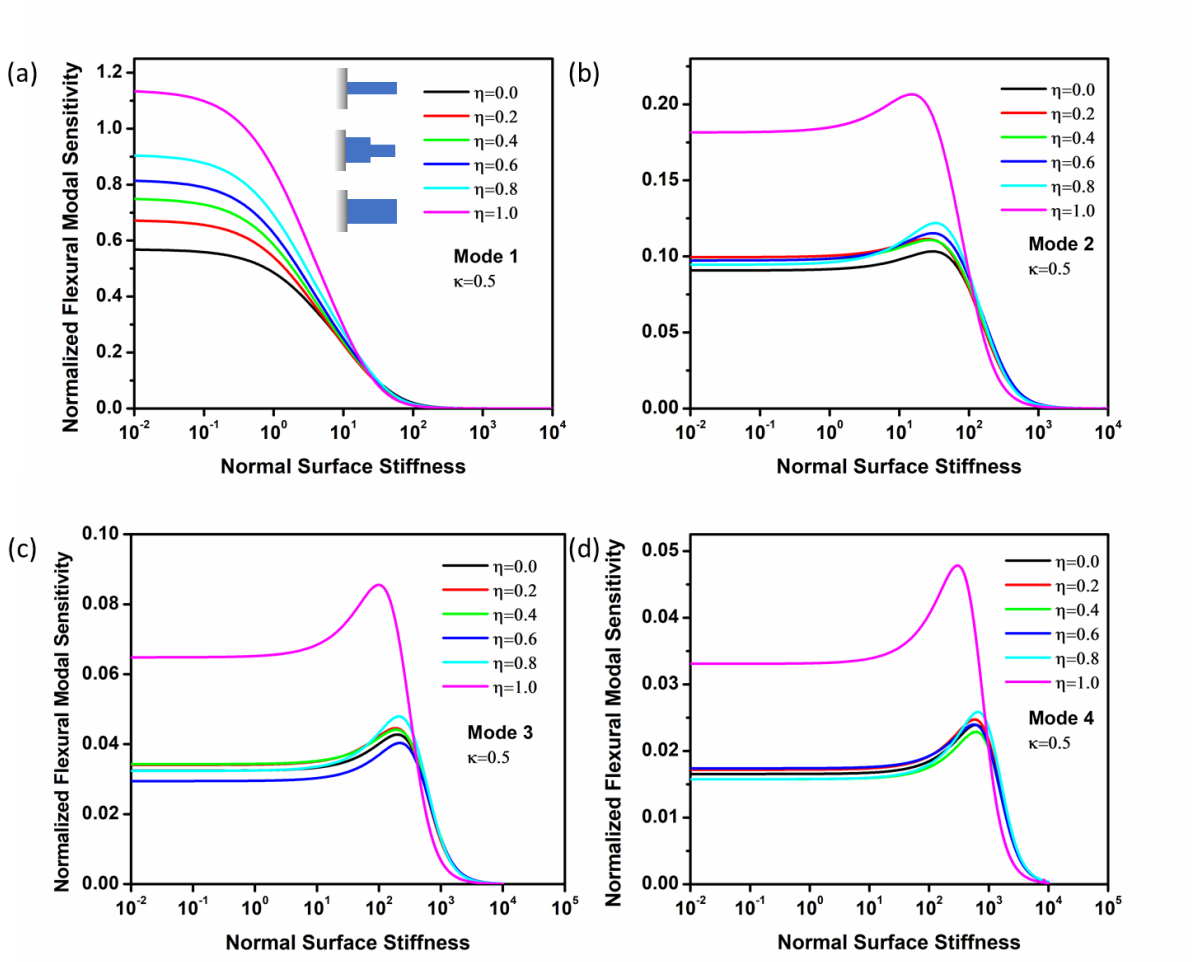

Figure 5. Flexural modal sensitivity of overhanging cantilever ($\kappa = 0.5$) as function of normal contact stiffness and overhanging length for a) first mode, b) second mode, c) third mode, and d) fourth mode.

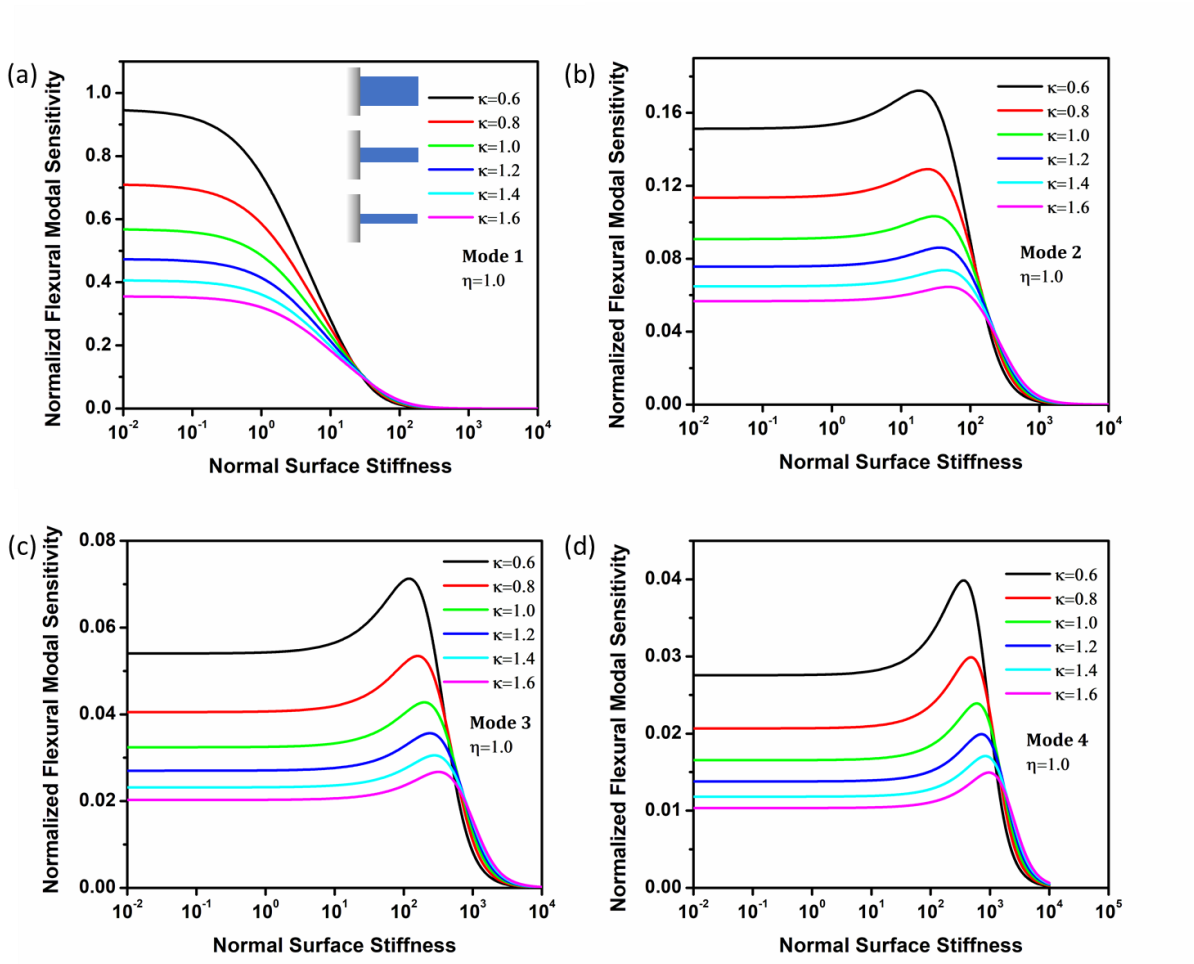

Figure 6. Flexural modal sensitivity of width-varying cantilevers with $\eta = 1$ as function of normal contact stiffness and overhanging width for a) first mode, b) second mode, c) third mode, and d) fourth mode.

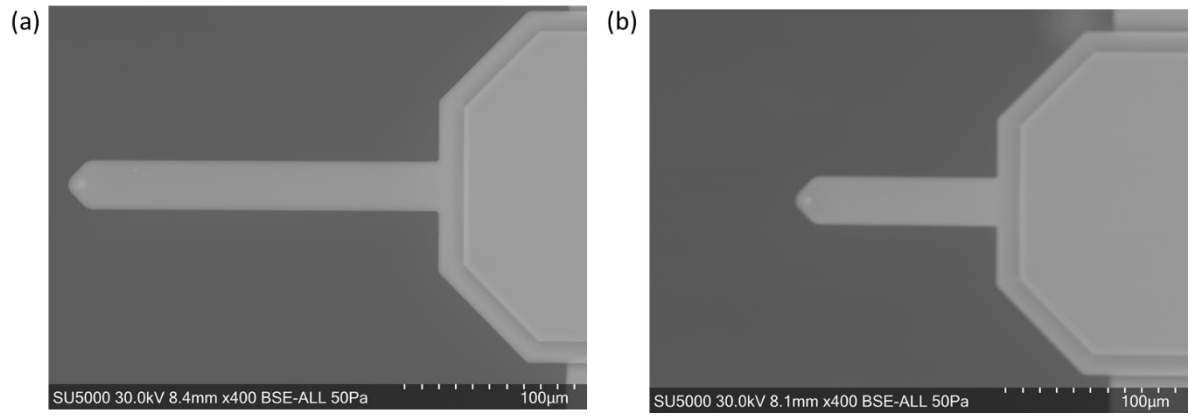

Figure 7. Representative scanning electron microscopy images of a) SCOUT70 and b) SCOUT350 cantilevers. The cantilevers are shown at 400× magnification. The manufacturer's specifications for the length, width, and thickness are 225, 30, and 2.5 µm for SCOUT70, and 125, 30, and 4.5 µm for SCOUT350, respectively.

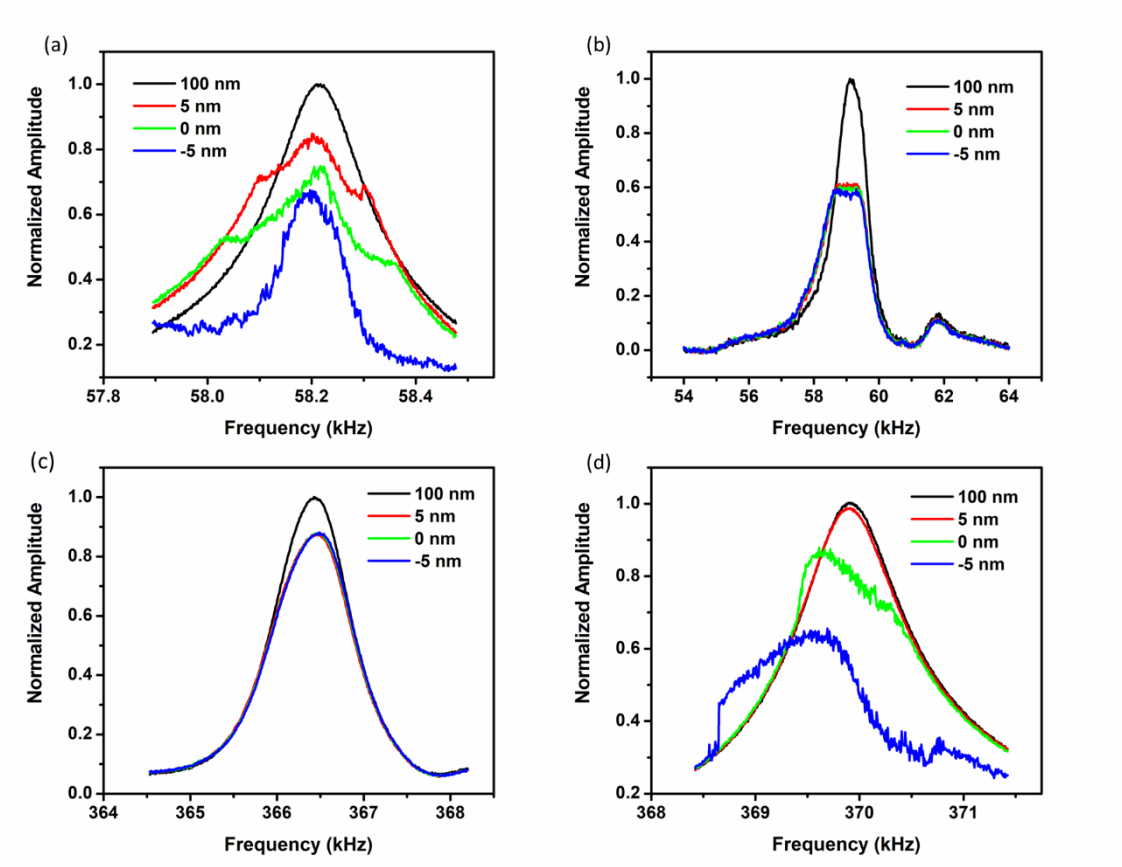

Figure 8. First-mode frequency response of a) SCOUT70 cantilever vs SE, b) SCOUT70 cantilever vs PS, c) SCOUT350 cantilever vs SE and d) SCOUT350 cantilever vs PS.

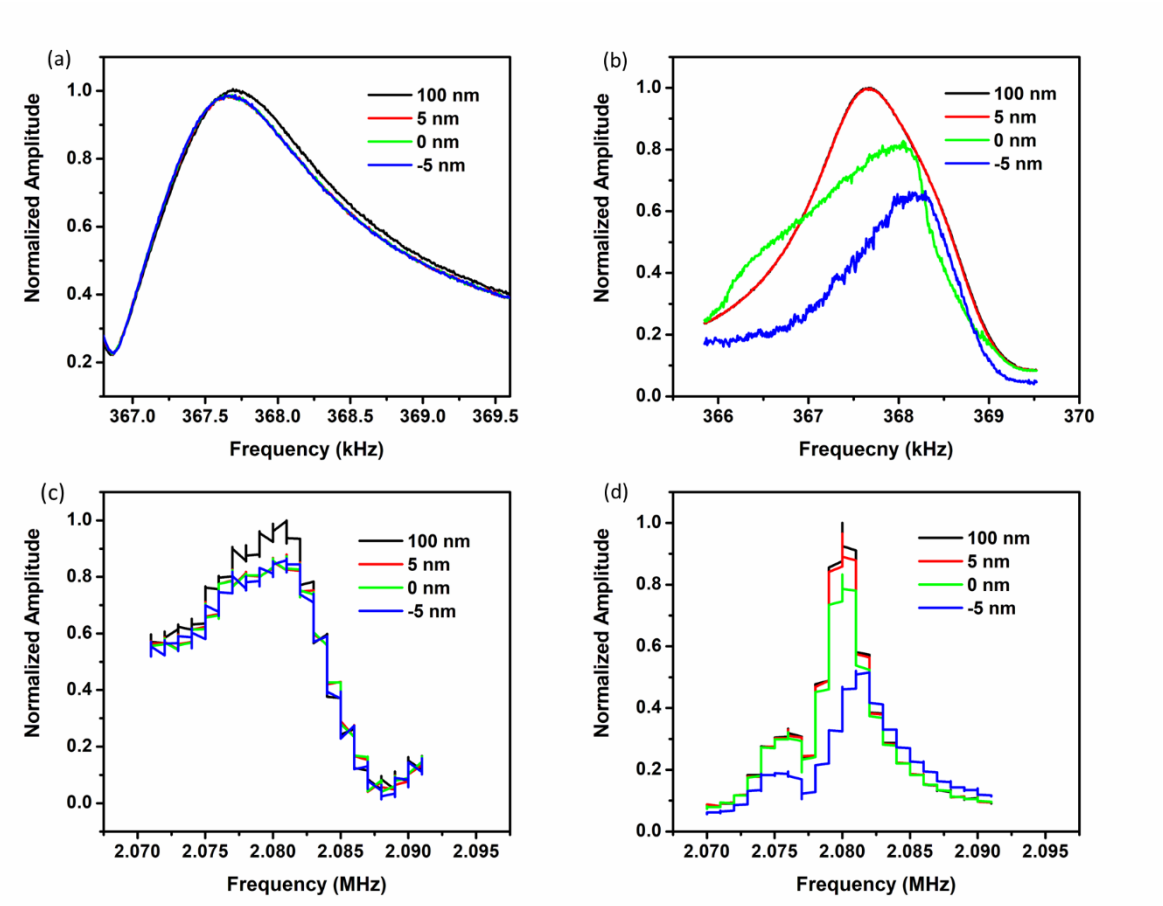

Figure 9. Second-mode frequency response of a) SCOUT70 cantilever vs SE, b) SCOUT70 cantilever vs PS, c) SCOUT 350 cantilever vs SE, and d) SCOUT350 cantilever vs PS.

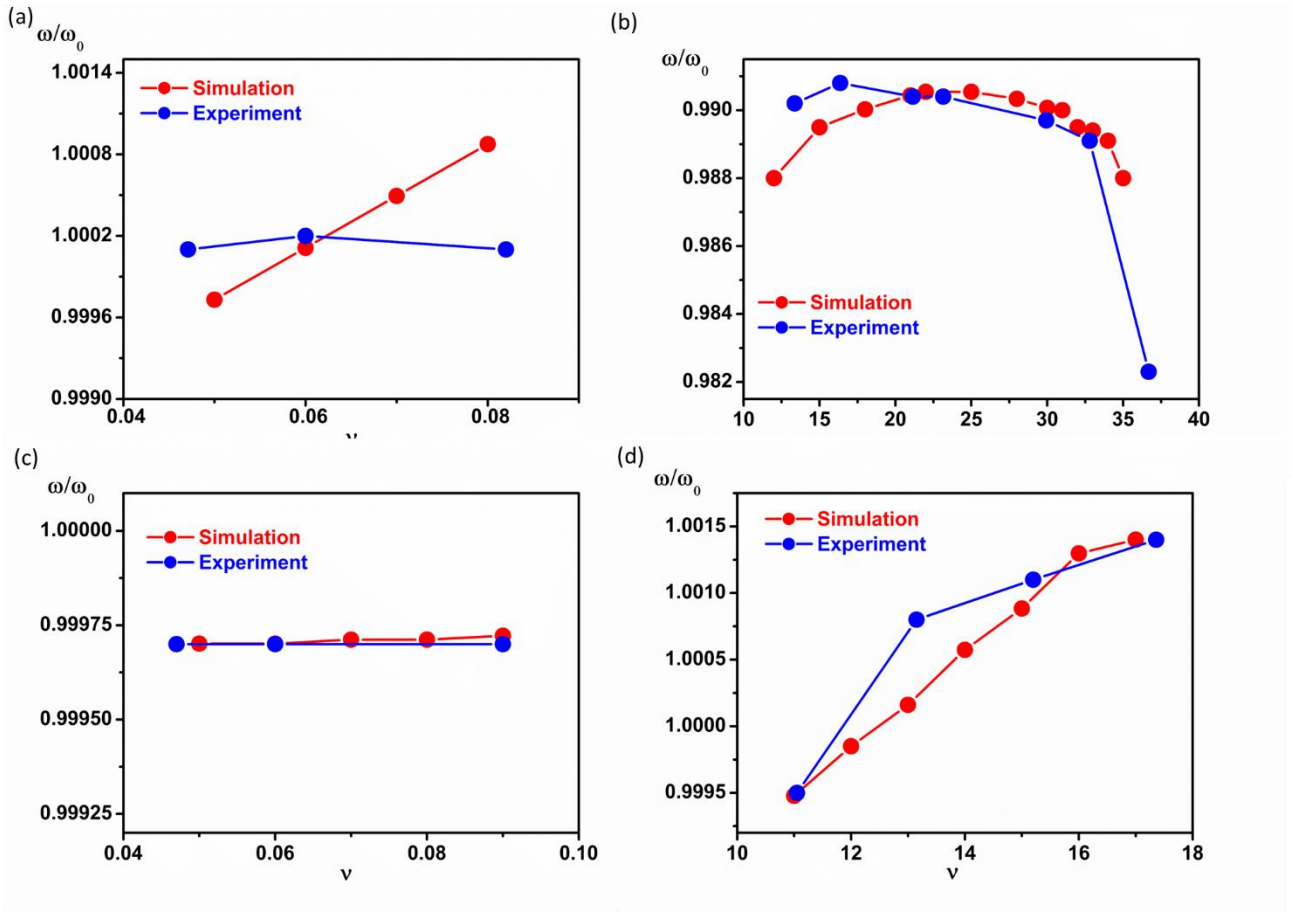

Figure 10. Comparison between simulation and experimental results for a) first-mode frequency response of SCOUT70 cantilever vs SE, b) first-mode frequency response of SCOUT70 cantilever vs PS, c) Second-mode frequency response of SCOUT70 cantilever vs SE, d) Second-mode frequency response of SCOUT70 cantilever vs PS.